The Laryngoscope

Anatomic Optical Coherence Tomography (aOCT) for Evaluation of the Internal Nasal Valve

Candace M. Waters, MD; Wesley H. Stepp, MD, PhD; Joseph Conduff, MD; Santosh Balakrishnan, PhD; Ruofei Bu, PhD; Amy L. Oldenburg, PhD; Julia S. Kimbell, PhD; William W. Shockley, MD; Joseph Madison Clark, MD

Objectives/Hypothesis: To establish the utility of anatomic optical coherence tomography (aOCT) in evaluating internal nasal valve (INV).

Study Design: Anatomic specimen imaging study.

Methods: Fresh-harvested human specimen heads were evaluated using both computed tomography (CT) imaging as well as using aOCT. Scans were performed at three time points: 1) After septoplasty for cartilage harvest, 2) after placement of butterfly graft (BFG), and 3) after placement of bilateral spreader grafts (SG). Imaging data were then converted into 3D models of the nasal airway. CT- and aOCT-generated models were compared by both static volumetric analysis and computational fluid dynamics (CFD) to predict nasal resistance and pressure.

Results: Scans using aOCT showed comparable results to CT in terms of volumetric parameters both before and after intervention. Analysis of aOCT data by CFD demonstrated decrease in pressure after SG or BFG intervention. No statistically significant difference was observed when comparing CT- and aOCT-generated calculations of pressure or resistance.

Conclusion: The INV can be imaged in a static fashion using aOCT technology. Advantages over traditional CT imaging include lack of exposure to radiation and rapid scan time. In addition, in-office use is possible as aOCT technology develops. Further investigation will be necessary to define the role of aOCT in the dynamic evaluation of this vital component of the nasal airway.

Key Words: Internal nasal valve, computational fluid dynamics, anatomic optical coherence tomography, rhinoplasty.

Level of Evidence: III

***Laryngoscope*, 00:1–9, 2021**

INTRODUCTION

The internal nasal valve (INV) plays an integral role in the common patient complaint of nasal airway obstruction (NAO). Level IV evidence including two systematic reviews suggest reduced nasal airflow resistance and improved patient satisfaction[1,2] after nasal valve repair (NVR). However, variations in technique have resulted in little higher-level evidence that describe when intervention is necessary and which method is most appropriate. The American Academy of Otolaryngology-Head and Neck Surgery released a Clinical Consensus Statement describing nasal valve compromise (NVC) as a "distinct and primary cause of symptomatic NAO."[3] Despite this statement, to date there is no consensus on which surgical approach offers better patient outcomes. Nor is there consensus on a standard objective assessment that could be used to compare various interventions performed by different surgeons.

The pursuit of the ideal method or surgical technique for the repair of NVC is ongoing and is the subject of active research at multiple institutions including our own.[1,2,4–15] Models using human anatomic specimens have been used to study objective measures of NVC by computed tomography (CT) and acoustic rhinometry,[16,17] while computational fluid dynamics (CFD) has evolved to become a reliable method for comparing resistance, heat flux, and nasal airway partitioning.[4,5,18–23] The foremost limitations of current CFD modeling are: 1) The use of CT with its inherent radiation risk as the basis for anatomic reconstruction, and 2) the inability of standard CT to capture the dynamic component of NVC. Although magnetic resonance imaging can also be used for CFD modeling, CT is the preferred imaging modality for airway reconstruction due to better clarity of the airway on images, lower cost, easier access, and faster speed of imaging. These limitations have prevented our group

From the Department of Otolaryngology–Head and Neck Surgery (C.M.W., W.H.S., J.C., J.S.K., W.W.S., J.M.C.), University of North Carolina at Chapel Hill, Chapel Hill, North Carolina, U.S.A.; Department of Otolaryngology–Head and Neck Surgery (C.M.W.), Wake Forest Baptist Medical Center, Winston-Salem, North Carolina, U.S.A.; and the Department of Physics (S.B., R.B., A.L.O.), University of North Carolina at Chapel Hill, Chapel Hill, North Carolina, U.S.A.

Editor's Note: This Manuscript was accepted for publication on November 29, 2021.

Portions of this research were presented at The Triological Society Meeting, January 2019, San Diego, California, U.S.A.

Research reported here was supported by the National Institutes of Health under award numbers R01 HL123557 and R01 HL154429. The content is solely the responsibility of the authors and does not necessarily represent the official views of the National Institutes of Health.

The authors have no other funding, financial relationships, or conflicts of interest to disclose.

Send correspondence to Joseph Madison Clark, MD, Campus Box# 7070, Chapel Hill, NC 27599. E-mail: madison_clark@med.unc.edu

DOI: 10.1002/lary.29979

from making the transition from the anatomic specimen experimental model to using CFD to study NVC differences in our patient population.

Optical coherence tomography (OCT) is an imaging method that generates cross-sectional images by measuring the magnitude and echo time delay of light backscattered from different depths in biological tissue. Anatomic Optical Coherence Tomography (aOCT) is a technological variant of OCT that is designed for volumetric imaging of the airways and features a longer imaging range than conventional OCT systems. The primary emphasis of the aOCT system is to image the airways with high resolution, to accurately reproduce the airway shape.[24,25] Owing to the use of low-coherence interferometry with near infrared light, this emerging imaging modality can capture dynamic changes in airway structures with no radiation exposure and with higher resolution than CT. In this study, we aim to validate and expand on prior work[4,26] by performing a study using single-surgical interventions on each human anatomic specimen and comparing anatomic reconstruction of the INV using aOCT to CT-based reconstructions using CFD as well as volumetric analysis. Each specimen was assessed by both aOCT and CT before and after receiving spreader grafts (SG) and a butterfly graft (BFG). Our primary outcome was to assess the ability of the aOCT-based INV reconstructions to show similar overall changes in nasal airway pressure and resistance to those of CT-based reconstructions following each intervention. We believe that by correlating the data obtained by aOCT and CT using CFD, we will determine whether a minimally interventional assessment (aOCT) will allow for meaningful comparison between two surgical alternatives while avoiding radiation exposure and allowing for future assessment of dynamic collapse of the INV.

MATERIALS AND METHODS

This study was deemed to be exempt from Institutional Review Board review based on the use of anatomic specimens only.

Surgical Procedures and Imaging

Four cadaveric heads (Caucasian; 2 male, 2 female; aged between 65 and 86 years) were obtained (Science Care Inc., Arizona) for study analysis. Initial examination of the nasal cavities was performed by senior surgeons (J.M.C. and W.W.S.) and septoplasty performed on 2 heads as clinically indicated by physical exam and for harvest of SG. Excess secretions were suctioned from the nose and nasopharynx of all heads prior to initial scan. Harvest of auricular cartilage was performed from 2 heads for creation of BFG.

Each head then underwent imaging via CT and aOCT modalities at each of three time-points: 1) "pre-intervention," which was following septoplasty in 2 heads; 2) after placement of bilateral SG via open approach; and 3) after placement of BFG via closed (intercartilaginous) approach. Two heads underwent SG followed by BFG, whereas the remaining 2 heads underwent BFG prior to SG. Grafts from primary intervention were removed prior to placement of grafts for secondary intervention. This alternating order approach was used to minimize potential bias from performing procedures in the same order on all heads. Graft placement was confirmed by senior surgeons prior to proceeding to imaging. After each procedure, the soft-tissue envelope was re-draped, all incisions were closed in standard fashion and both CT and aOCT scans were repeated. Treatment order matrix can be seen in Table I.

CT scans were obtained using 3-D Accuimoto F170 cone beam CT system (J. Morita Mfg. Corp., Japan). Settings for CT scanning included 0.33 mm pixels and 0.66 mm increments. aOCT scans of the INV were obtained, using a system described previously,[26] separately for each side of the airway using a 143 cm-long fiber-optic probe with a side-looking beam. To protect the probe, it was passed through a fixed transparent sheath during scanning. Helical scans were performed (rotation: 20 Hz, translation: 6 mm/s) during retraction of the probe through the sheath for a distance of ~20 mm. Placement of the probe in the nasal cavity was performed by coupling the sheath-probe system to a 0-degree endoscope (diameter 4 mm, length 18 cm; Karl Storz SE & Co., Germany). This endoscopic video confirmation of placement was supplemented by reviewing real-time aOCT images.[26] Details of the experimental setup for aOCT acquisition are shown in Figure 1.

Nasal Model Construction

CT reconstructions. CT scans were converted to 3D reconstructions of the nasal airway via Mimics medical imaging software (Mimics™, version 18.0; Materialize, Inc., Plymouth, Michigan). A threshold was selected to delineate the nasal airways (−1,024 to −300 Houndsfield units) for all CT models. Each reconstruction then underwent selective hand editing to confirm that the generated airway was anatomically accurate based on physician review of the CT images, and to remove the paranasal sinuses. Pre-intervention reconstructions were created first to produce a complete reconstruction of the airway extending from the nasal vestibule through the nasopharynx (Fig. 2A,B). Post-intervention reconstructions after SG and BFG were generated in a similar fashion but confined to the nasal airway anterior to the nasion. The reconstructions were thus truncated to confine the observed differences in computed airflow patterns to the area of surgical intervention. CT reconstructions from interventions were aligned with the pre-intervention airway using algorithms created from bony landmark alignment. Post-SG and post-BFG reconstructions were then merged with the posterior portion of the pre-intervention airway to create a complete CT-generated reconstruction of the airway for CFD analysis (Fig. 2C). This process generated 3 CT-based reconstructions (pre-intervention, post-SG, and post-BFG) for each of the four specimens for a total of 12 CT-based reconstructions.

aOCT reconstructions. The aOCT data were segmented, resampled into a 3D reconstruction, and imported into Mimics™ for further assessment of each INV. These were aligned with the 3D reconstructions from the CT images generated above. Resampling of the CT images was necessary to

TABLE I.
Treatment Order Matrix for Cadaver Study.

ID	Intervention 1	Intervention 2	Septoplasty?
Head 01	SG (bilateral)	BFG	Y
Head 02	SG (bilateral)	BFG	N
Head 03	BFG	SG (bilateral)	Y
Head 04	BFG	SG (bilateral)	N

BFG = butterfly graft; SG = spreader grafts.

reconstruct in a plane perpendicular to the nasal dorsum. This plane is commonly used in the assessment of the INV as it closely approximates the direction of airflow.[27,28] CT scan reconstructions were then truncated to match the limits of the aOCT beam. Thus, we created a "segment" of each CT-generated airway that overlapped the 20 mm-long capture of the analogous aOCT reconstruction. Details of alignment, resampling, reconstruction, and trimming are beyond the scope of this manuscript but can be found in our separately-published aOCT technique article.[26] As multiple aOCT scans were performed of each side at each time point, the most accurate reconstruction was selected based on review of the airway models compared to CT models.

Volume data were acquired from the matched reconstructions to compare the volume of the INV as captured by CT vs. aOCT at each intervention. Next, the CT and aOCT "segments" created were imported into the full composite airway reconstructions. Standardized alignment was performed and confirmed. The Boolean Operations function in Mimics™ was used to subtract the CT "segment" from the corresponding CT airway reconstruction and the aOCT "segment" for the same intervention was merged in to create a hybrid reconstruction with the aOCT-generated INV (Fig. 3A). Views of paired INV "segments" from CT and aOCT data in multiple orientations can be found in Figure 3B. This process generated 3 hybrid aOCT-CT reconstructions (pre-intervention, post-SG, and post-BFG) for each specimen for a total of 12 hybrid aOCT-CT reconstructions.

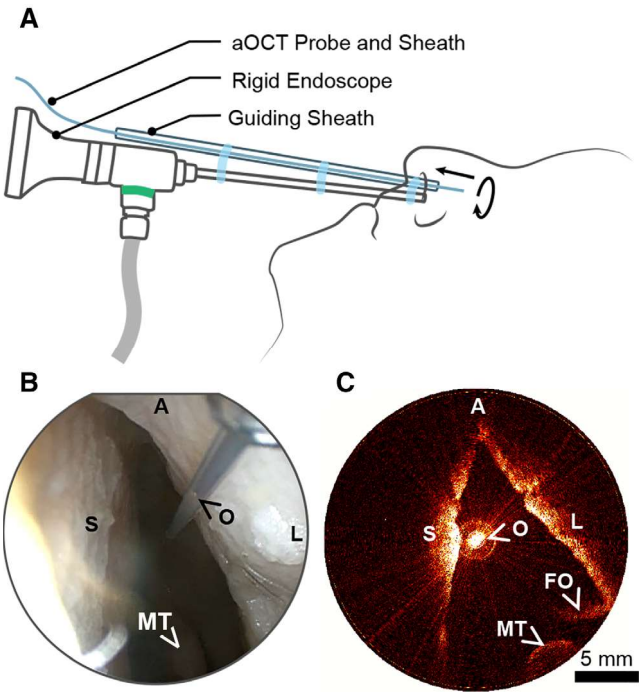

Fig. 1. A, Rendering of setup used to perform anatomic optical coherence tomography (aOCT) imaging of the nasal airways. B, Representative nasal endoscopy image depicting the positioning of the aOCT probe and sheaths in the left nasal cavity. C, Representative aOCT image acquired in left nasal cavity of the same patient. O: aOCT probe tip within protective guiding sheath; MT: middle turbinate; L: lateral nasal wall; S: septum; A: apex of INV; FO: fold-over/aliasing artifact from nasal structures beyond the maximum imaging radius (12 mm) of aOCT. Reprinted with permission from Balakrishnan et al.[26] [Color figure can be viewed in the online issue, which is available at www.laryngoscope.com.]

CFD analysis. The completed reconstructions were exported from Mimics™ and imported into computer-aided design and meshing software (ICEM-CFD™, version 15.0; ANSYS, Inc., Lebanon, New Hampshire). Meshing and CFD simulation of

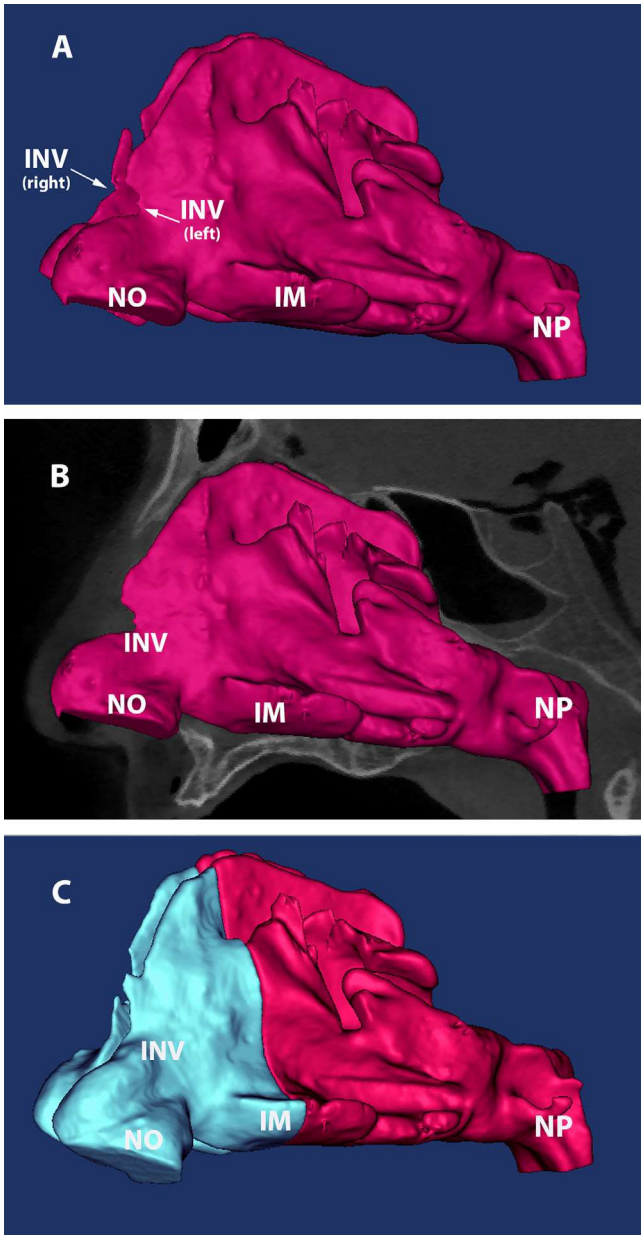

Fig. 2. A,B Pre-intervention airway model generated from computed tomography (CT) data. Model extends from nasal vestibule through nasopharynx. Paranasal sinuses have been removed. A, Full airway model as viewed from left in parasagittal orientation. B, Model superimposed on sagittal cut CT scan for anatomic orientation. C, Composite CT-generated airway model (example from butterfly graft [BFG] intervention). Airway generated from post-intervention CT data were aligned with the pre-intervention airway using algorithms created from bony landmark alignment. Post-intervention model of anterior airway (blue) was then merged with the posterior portion of the pre-intervention airway (pink) to create a complete CT-generated model of the airway for Computational fluid dynamics analysis. INV = internal nasal valve; IM = inferior meatus; NO = nostril; NP = nasopharynx. [Color figure can be viewed in the online issue, which is available at www.laryngoscope.com.]

airflow were performed as described in our previous work.[4] Briefly, meshes consisting of approximately 4 million tetrahedral elements with quality ≥0.3 were created using ICEM-CFD™, including the addition of a 3-cm-long outlet tube to the nasopharynx to improve fully-developed flow approximation at the outlet. Airflow simulations at a steady, inspiratory flow rate of 15 L/min under pressure-driven, laminar conditions were conducted with CFD software (Fluent™, version 18.1; ANSYS, Inc.). Pressure boundary conditions consisted of setting static pressure to 0 at the nostrils and a negative value at the outlet fitted to produce a 15 L/min total volumetric flow rate in each model (range: −11.45 to −2.22 Pa). Volumetric flow rate (Q) in ml/sec and the drop in average static pressure (ΔP) in Pascals (Pa) from the nostrils to a coronal plane slightly anterior to the choanae were calculated for each nasal side using Fluent. Nasal resistance in Pa/(ml/sec) was computed for each side as $\Delta P/Q$. Our previous work suggested a lack of sensitivity of wall shear stress to NAO surgery[19] and higher sensitivity of pressure and resistance than heat flux to NVR when assessing the INV alone,[4] so wall shear and heat transfer analyses were omitted from the current study.

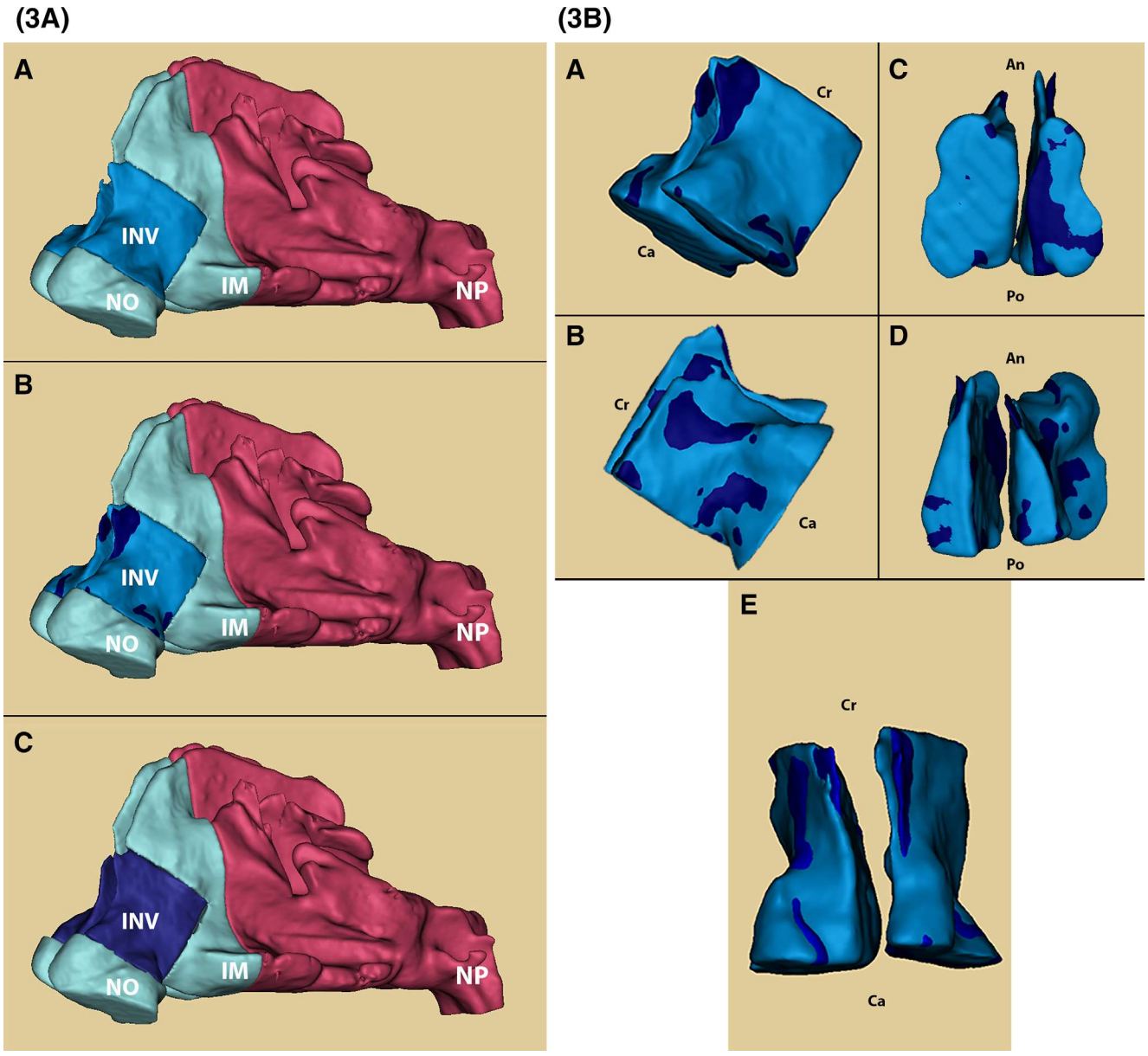

Fig. 3. A, Creation of anatomic optical coherence tomography (aOCT)-hybrid airways by merging data. a, Composite airway model with computed tomography (CT)-based internal nasal valve (INV) area highlighted. b, Model with CT-based and aOCT-based INV "segments" overlapped. c, Model with aOCT-based INV "segment" replacing CT-based INV. All models for this figure are examples from a post-butterfly graft (BFG) intervention. IM = inferior meatus; NO = nostril; NP = nasopharynx. B, Paired INV "segments" from post-BFG intervention with full airway removed. Light blue: CT-generated data. Dark blue: aOCT-generated data. a, Lateral view from left (analogous to previous figures). b, Lateral view from right. c, Cranio-caudal view from caudal end. d, Cranio-caudal view from cranial end. e, Antero-posterior view from above. An = anterior; Ca = caudal; Cr = cranial; Po = posterior. [Color figure can be viewed in the online issue, which is available at www.laryngoscope.com.]

Statistical analysis

Ratio-paired Student's *t*-tests were used for comparisons between CT and aOCT-CT hybrid model groups, and among interventions within the CT and aOCT-CT hybrid model groups. One-way analysis of variance was used to compare group means for all six model groups (CT-based pre-intervention, CT-based post-SG, CT-based post-BFG, aOCT-CT hybrid pre-intervention, aOCT-CT hybrid post-SG, and aOCT-CT hybrid post-BFG). Statistical significance was associated with two-sided p-values less than 0.05.

RESULTS

Volumetric Analysis

Volumes of the airway at the INV as measured by CT and aOCT were calculated from pre-intervention specimens. Left and right sides were analyzed separately. There was no significant difference between aOCT and CT-derived volumes of the INV for either left or right nasal airways ($P = .763$, left; $P = .745$, right) (Fig. 4A). Next, we analyzed the percent change in volume from pre-operative values after each intervention (BFG and SG) using both imaging modalities. There was no significant difference in the percent change in volume calculated using CT as compared to aOCT analysis for either SG (Fig. 4B) or BFG (Fig. 4C), regardless of laterality.

CFD Analysis

CFD estimates of pressure and resistance were generated for each side of the nose using each imaging modality. Similar trends were observed with both parameters between aOCT and CT data (Fig. 5A). Pressure on each side of the nose showed trends toward decreasing after SG intervention with either modality, although these did not reach statistical significance with CT-based imaging (Fig. 5A, left). Pressure on each side of the nose showed a statistically significant decrease after BFG using CT data, while aOCT data demonstrated statistically significant decrease in airway pressure for both SG and BFG versus pre-operative controls (Fig. 5A). There was no consistent statistically significant difference in resistance in either nasal airway using either modality, though SG and BFG did demonstrate significance using CT- and aOCT-based imaging respectively (Fig. 5B).

Total nasal resistance showed statistically significant difference between pre-op and SG with CT-generated data ($P < .05$). Difference in total nasal resistance between pre-op and BFG approached statistical significance using CT-generated data ($P = .051$) (Fig. 5B). Neither SG nor BFG showed statistically significant improvement in left-sided airway resistance when analyzed using aOCT-generated data though right-sided resistance improved significantly when analyzed by aOCT (Fig. 5B). Additionally, total airway resistance generated by each imaging modality showed similar trends were observed between CT and aOCT (Fig. 5C). There was no significant difference between the two modalities for any individual intervention.

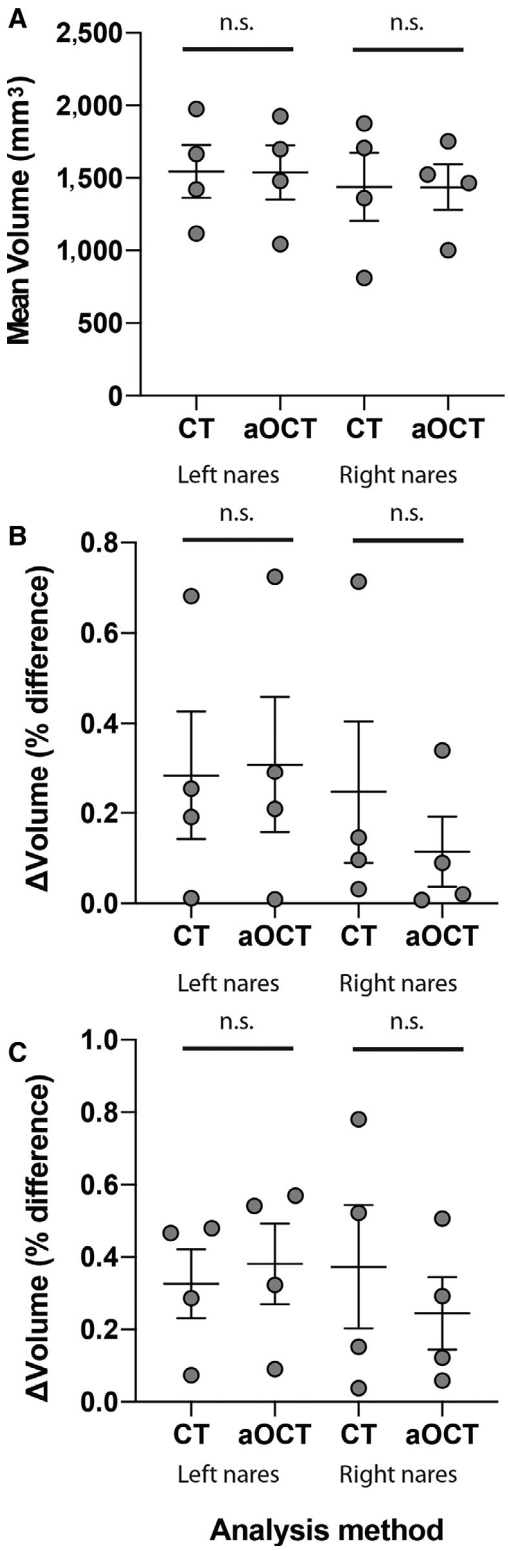

Fig. 4. Volumetric analysis of computed tomography (CT)-generated and aOCT-generated airways at the internal nasal valve. A, Computational fluid dynamics-derived volumes of the bilateral nasal airways between two imaging modalities (CT and aOCT). Percent change in static airway volume following spreader graft (B) and butterfly graft (C) of the left and right nasal airways using both CT and aOCT imaging modalities. Error bars demonstrate ± the standard error of the mean (SEM). aOCT = anatomic optical coherence tomography; n.s. = not statistically significant.

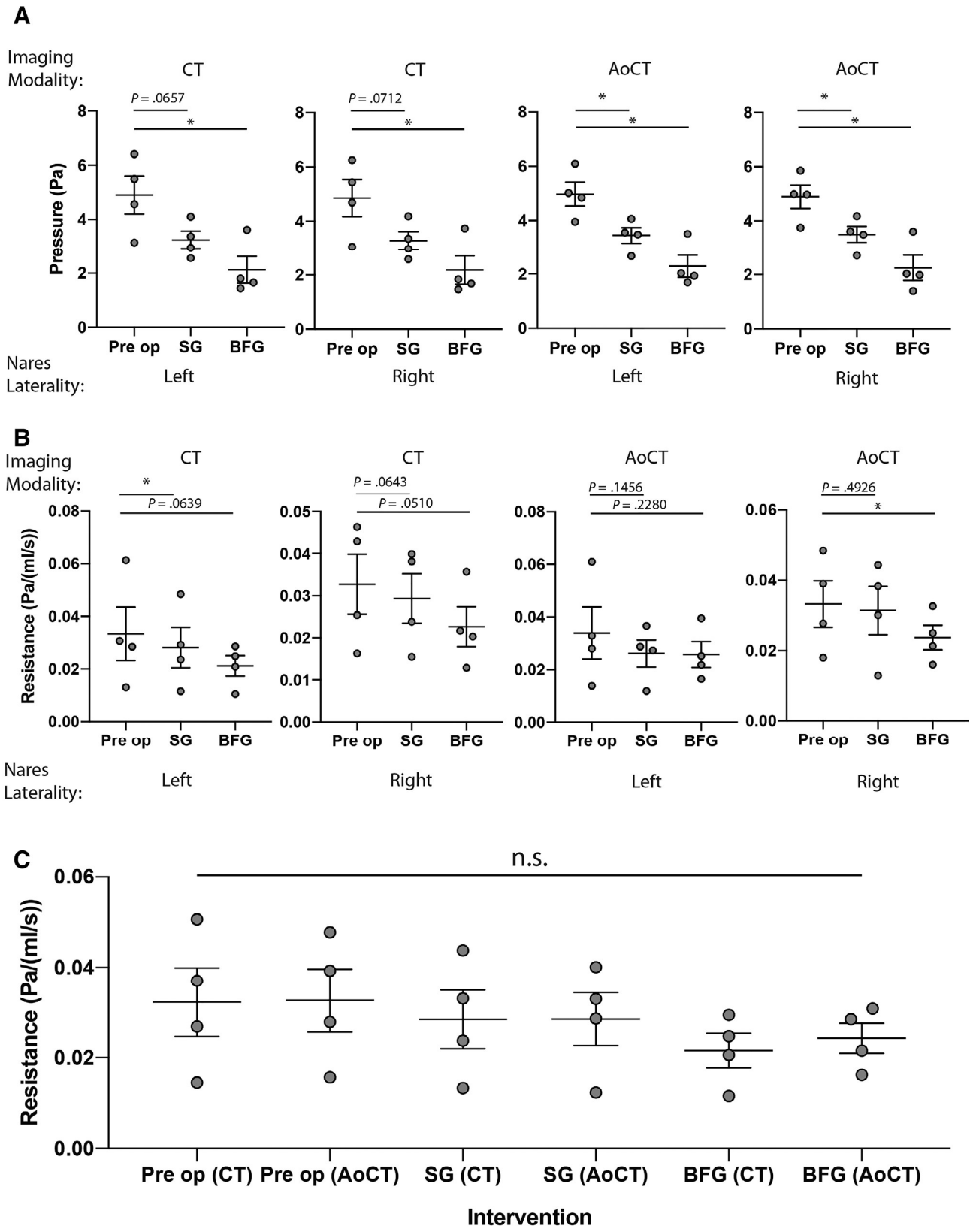

Fig. 5. Computational fluid dynamics (CFD) analysis of pressure and nasal resistance using dual imaging modalities. A, CFD-derived pressure analysis of the bilateral nasal airways pre- and postsurgical intervention with spreader graft (SG) (short line) and butterfly graft (BFG) (long line). B, CFD-derived calculations for bilateral nasal airway resistance pre- and post-surgical intervention with SG and BFG. C, Combined nasal airway resistance calculations comparing dual imaging modalities. Error bars represent ± the SEM. *$P < .05$; n.s. = not statically significant.

DISCUSSION

While NVC can result from impairment of either the INV or the external nasal valve, the INV is most often targeted for surgical intervention, as it forms the narrowest part of the nasal airway.[7] Located at the junction of the caudal aspect of the upper lateral cartilage, septum and caudal head of the inferior turbinate, small changes in this region can generate exponential changes in nasal airflow.

NVC generally results from one of two different causes: Static obstruction and dynamic collapse of the airway, either alone or in combination. Traditional surgical interventions for correcting NAO were typically targeted at improving static obstruction by increasing the cross-sectional area of the nasal valve region. These interventions include septoplasty, inferior turbinate reduction, and SG. More recent techniques address both static and dynamic collapse in NVC. These include butterfly graft, spreader flaps, and various combination techniques with batten grafts (paired with SG, lateral crural strut grafts, or flaring sutures). A reliable, objective method to compare the various techniques remains elusive.

Recently, our group published data comparing SG and BFG for repair of INV in human anatomic specimens.[4,22] Similar to the current study, each head underwent CT evaluation before and after both SG and BFG placement, and we utilized CFD based on nasal airway models reconstructed from the CT images. The benefit of CFD is its ability to assess nasal airway resistance and heat flux (a measure of mucosal cooling), which are CFD biophysical variables strongly correlated with patient-reported symptoms.[19,21,23] We demonstrated that nasal airway resistance was consistently improved in specimens that had butterfly graft placement, independent of the need for septoplasty or the order in which the surgical interventions were performed.[4]

In contrast, the present study represents a proof of concept using aOCT in a human anatomic specimen model, comparing it to CT using both volumetric and CFD analysis. In the study design, we repeated the methods used previously to compare two surgical modalities (SG and butterfly grafts). Replicating the methods allows direct comparison to that study, providing additional validity to our assessment of aOCT as a minimally invasive substitute for CT in CFD analysis of the INV. This study focused on demonstrating the ability of aOCT to evaluate the anatomy of nasal valve accurately with respect to static shape and functionality. The major advancement of this study over our previous work was the use of INV reconstructions based on aOCT imaging technology. The key outcome of this study was that models with aOCT-based reconstructions produced results that were similar to CT-based results. The addition of CFD analysis allows improved assessment of the functional component of nasal anatomy. Next steps will be evaluation of the dynamic imaging capabilities of aOCT to diagnose and discern treatment modalities for NVR. These next steps involve patient recruitment and in vivo utilization of aOCT technology, for which the ex vivo methods testing and validation of the present study are necessary. Our current study is critical to gaining justification for IRB approval for future investigation. Future utilization of the dynamic imaging capabilities of aOCT will provide a method for capturing movement of the nasal sidewall or dynamic nasal sidewall collapse and allow objective comparison of various methods of NVR.[26]

Ultimately, CFD analysis could be performed using aOCT alone, although current limitations of the technology precluded creation of a full airway model from aOCT data for this study. Because the posterior nasal airway and nasopharynx were not manipulated with placement of SG or butterfly grafts, and all cadaveric specimens suffered degradation over the course of the day of interventions and scans, our use of posterior airway reconstructions from pre-intervention CT scans in all models provided more accurate representations of the airways. In addition, differences in results among cases could be ascribed solely to each intervention.

We have demonstrated previously that the butterfly graft has more consistent reduction in nasal airway resistance than SG, and it is more effective achieving equivalent airflow allocation between the nasal airways.[4] In this study, we show trends consistent with our prior findings, though without statistically significant improvement in nasal airway resistance following butterfly graft placement by either imaging modality. We surmise that the difference from our previous study results stems from the inability to select for INV pathology in our cadaveric models, as patient selection is key in determining appropriate intervention for NVR in the clinical setting. However, we demonstrate no statistically significant differences between CT and aOCT imaging modalities with direct comparison of calculated resistance for each intervention (Fig. 5C). Both modalities demonstrated a statistically significant decrease in pressure between pre-op and post-BFG interventions. When comparing pressure between pre-op and post-SG, only aOCT trended toward significance.

Heat flux and airway resistance have been shown to correlate with patient-reported outcome measures (PROMs) of subjective nasal patency.[19,23,29] While this study was performed with tissue specimens lacking the resiliency of live tissue, we did see a statistically significant reduction in nasal airflow resistance after SG and lower resistance with BFG that trended toward significance. These trends were also present in our aOCT data but did not reach statistical significance. Future work using aOCT-based CFD with patients following surgical interventions could further clarify the impact that those interventions have on objective measures (e.g. heat flux and nasal airflow resistance) as well as PROMs.

One of the major limitations of this study is the small number of specimens used in this study, which was necessary for two reasons. First, preserved calvaria are difficult to obtain and it is prohibitively expensive to use more than is required for statistical analysis. Second, the surgical procedures and computer modeling process required dozens of person-hours for the analysis of a single head. Therefore, the feasibility of bringing the study to completion before tissue degradation and cost became unrealistically decreased as the number of specimens

increased. However, the veracity of our current findings is supported by consistent agreement among multiple, independent studies. We also recognize the limitations of aOCT in these scenarios, specifically the narrow imaging plane inside the nose. We focused our aOCT scans at the INV to image the portion of the airway targeted by our surgical interventions. We then combined this aOCT-imaged airway with its CT-imaged counterpart to create a complete model the entire airway, making radiation exposure necessary for this CFD study. However, the usefulness of aOCT is not limited to its ability to fit within a CFD framework. Creation of pre- and postoperative models of the INV itself would be useful for evaluation of surgical treatment or to stratify between treatments, and could be accomplished with current aOCT technology and thus without radiation. Evolution of the aOCT technology will ideally enable imaging of the entire airway.

We have previously reported results from this study design in terms of anatomic similarity between computed INV models generated by aOCT and CT.[26] In contrast, results reported here allow us to analyze the function of the INV within the context of the nasal airway as a whole, rather than modeling this small segment of the nasal anatomy in isolation. Furthermore, CFD analysis enables the measurement of pressure and resistance, which are more clinically relevant than changes in volume alone.

CONCLUSION

Taken together, the findings in this study show that aOCT is comparable to CT in data acquisition for CFD analysis, at least in preserved calvaria. By volumetric analysis, morphologic comparison, and calculated resistance, aOCT showed good fidelity in creating INV models that mimic those generated by CT imaging. Therefore, we hope that with additional strides in aOCT technology we will be able to evaluate the nasal airway (particularly the INV) while avoiding the radiation exposure of CT-based imaging.

Furthermore, this study demonstrated the utility of aOCT as a promising modality for capturing real-time objective data comparing INV interventions. Our findings demonstrate that aOCT holds great promise to provide objective and precise methods for evaluating static and dynamic INV collapse, while obviating the need for ionizing radiation. Potential future directions for this technology would include in-office assessment of the INV to diagnose NVC and intraoperative assessment of graft placement.

Acknowledgments

The authors thank Bryan Brandon, MD and Meghan Norris, MS for their assistance during the surgeries and initial imaging scans.

Author Contributions

C.M.W., MD: Study design, Execution of cadaveric surgeries and scanning, Computer modeling, Data analysis, Manuscript preparation. W.H.S., MD, PhD: Study design, Execution of cadaveric surgeries and scanning, Computer modeling, Data analysis, Manuscript preparation. J.C., MD: Computer modeling, Data analysis, Manuscript preparation. S.B., PhD: Study design, Execution of cadaveric scanning, Computer modeling, Data analysis, Manuscript preparation. R.B., PhD: Study design, Execution of cadaveric scanning, Computer modeling, Data analysis, Manuscript preparation. A.L.O., PhD (Senior faculty advisor for aOCT lab): Study design, Computer modeling, Data analysis, Manuscript preparation. J.S.K., PhD (Senior faculty advisor for CFD lab): Study design, Execution of cadaveric scanning, Computer modeling, Data analysis, Manuscript preparation. W.W.S., MD (Co-Senior Author): Study design, Execution of cadaveric surgeries and scanning, Manuscript preparation. J.M.C., MD (Co-Senior Author; Corresponding Author): Study design, Execution of cadaveric surgeries and scanning, Manuscript preparation. All co-authors have reviewed and approved of the manuscript prior to submission.

BIBLIOGRAPHY

1. Rhee JS, Arganbright JM, McMullin BT, Hannley M. Evidence supporting functional rhinoplasty or nasal valve repair: a 25-year systematic review. *Otolaryngol Head Neck Surg* 2008;139:10–20.
2. Spielmann PM, White PS, Hussain SS. Surgical techniques for the treatment of nasal valve collapse: a systematic review. *Laryngoscope* 2009;119: 1281–1290.
3. Rhee JS, Weaver EM, Park SS, et al. Clinical consensus statement: diagnosis and management of nasal valve compromise. *Otolaryngol Head Neck Surg* 2010;143:48–59.
4. Brandon BM, Austin GK, Fleischman G, et al. Comparison of airflow between spreader grafts and butterfly grafts using computational flow dynamics in a cadaveric model. *JAMA Facial Plast Surg* 2018;20: 215–221.
5. Brandon BM, Stepp WH, Basu S, et al. Nasal airflow changes with bioabsorbable implant, butterfly, and spreader grafts. *Laryngoscope* 2020; 130:E817–E823.
6. Barrett DM, Casanueva FJ, Cook TA. Management of the nasal valve. *Facial Plast Surg Clin North Am* 2016;24:219–234.
7. Clark JM, Cook TA. The 'butterfly' graft in functional secondary rhinoplasty. *Laryngoscope* 2002;112:1917–1925.
8. Hassanpour SE, Heidari A, Moosavizadeh SM, Tarahomi MR, Goljanian A, Tavakoli S. Comparison of aesthetic and functional outcomes of spreader graft and autospreader flap in rhinoplasty. *World J Plast Surg* 2016;5: 133–138.
9. Helal MZ, El-Tarabishi M, Magdy Sabry S, et al. Effects of rhinoplasty on the internal nasal valve: a comparison between internal continuous and external perforating osteotomy. *Ann Plast Surg* 2010;64:649–657.
10. Howard BE, Clark JM. Evolution of the butterfly graft technique: 15-year review of 500 cases with expanding indications. *Laryngoscope* 2019;129: S1–S10.
11. Hurbis CG. An adjustable, butterfly-design, titanium-expanded polytetrafluoroethylene implant for nasal valve dysfunction: a pilot study. *Arch Facial Plast Surg* 2006;8:98–104.
12. Jalali MM. Comparison of effects of spreader grafts and flaring sutures on nasal airway resistance in rhinoplasty. *Eur Arch Otorhinolaryngol* 2015; 272:2299–2303.
13. Omranifard M, Abdali H, Rasti Ardakani M, Ahmadnia A. Comparison of the effects of spreader graft and overlapping lateral crural technique on rhinoplasty by rhinomanometry. *World J Plast Surg* 2013;2:99–103.
14. Reiffel AJ, Cross KJ, Spinelli HM. Nasal spreader grafts: a comparison of medpor to autologous tissue reconstruction. *Ann Plast Surg* 2011;66: 24–28.
15. Stacey DH, Cook TA, Marcus BC. Correction of internal nasal valve stenosis: a single surgeon comparison of butterfly versus traditional spreader grafts. *Ann Plast Surg* 2009;63:280–284.
16. Bae JH, Most SP. Cadaveric analysis of nasal valve suspension. *Allergy Rhinol* 2012;3:e91–e93.
17. Coan BS, Neff E, Mukundan S, Marcus JR. Validation of a cadaveric model for comprehensive physiologic and anatomic evaluation of rhinoplastic techniques. *Plast Reconstr Surg* 2009;124:2107–2117.
18. Garcia GJ, Rhee JS, Senior BA, Kimbell JS. Septal deviation and nasal resistance: an investigation using virtual surgery and computational fluid dynamics. *Am J Rhinol Allergy* 2010;24:e46–e53.

19. Kimbell JS, Frank DO, Laud P, Garcia GJM, Rhee JS. Changes in nasal airflow and heat transfer correlate with symptom improvement after surgery for nasal obstruction. *J Biomech* 2013;46:2634–2643.
20. Otto BA, Li C, Farag AA, et al. Computational fluid dynamics evaluation of posterior septectomy as a viable treatment option for large septal perforations. *Int Forum Allergy Rhinol* 2017;7:718–725.
21. Radulesco T, Meister L, Bouchet G, et al. Correlations between computational fluid dynamics and clinical evaluation of nasal airway obstruction due to septal deviation: an observational study. *Clin Otolaryngol* 2019;44: 603–611.
22. Shadfar S, Shockley WW, Fleischman GM, et al. Characterization of postoperative changes in nasal airflow using a cadaveric computational fluid dynamics model supporting the internal nasal valve. *JAMA Facial Plast Surg* 2014;16:319–327.
23. Sullivan CD, Garcia GJ, Frank-Ito DO, Kimbell JS, Rhee JS. Perception of better nasal patency correlates with increased mucosal cooling after surgery for nasal obstruction. *Otolaryngol Head Neck Surg* 2014;150: 139–147.
24. Armstrong JJ, Leigh MS, Sampson DD, Walsh JH, Hillman DR, Eastwood PR. Quantitative upper airway imaging with anatomic optical coherence tomography. *Am J Respir Crit Care Med* 2006;173:226–233.
25. Balakrishnan S, Bu R, Iftimia N, Price H, Zdanski C, Oldenburg AL. Combined anatomical optical coherence tomography and intraluminal pressure reveal viscoelasticity of the in vivo airway. *J Biomed Opt* 2018;23:1–4.
26. Balakrishnan S, Bu R, Waters C, et al. Utility of endoscopic anatomical optical coherence tomography in functional rhinoplasty. *J Biomed Opt* 2020;25:1–11.
27. Bloom JD, Sridharan S, Hagiwara M, Babb JS, White WM, Constantinides M. Reformatted computed tomography to assess the internal nasal valve and association with physical examination. *Arch Facial Plast Surg* 2012;14:331–335.
28. Suh MW, Jin HR, Kim JH. Computed tomography versus nasal endoscopy for the measurement of the internal nasal valve angle in Asians. *Acta Otolaryngol* 2008;128:675–679.
29. Zhao K, Blacker K, Luo Y, Bryant B, Jiang J. Perceiving nasal patency through mucosal cooling rather than air temperature or nasal resistance. *PLoS One* 2011;6:e24618.